Impact of spin-orbit currents on the electroweak skin of neutron-rich nuclei

C. J. Horowitz and J. Piekarewicz

Impact of spin-orbit currents on the electroweak skin of neutron-rich nuclei

C. J. Horowitz*

Center for Exploration of Energy and Matter and Department of Physics,
Indiana University, Bloomington, IN 47405, USA

J. Piekarewicz†

Department of Physics, Florida State University, Tallahassee, FL 32306, USA

(Dated: October 3, 2012)

Background: Measurements of neutron radii provide important constraints on the isovector sector of nuclear density functionals and offer vital guidance in areas as diverse as atomic parity violation, heavy-ion collisions, and neutron-star structure. **Purpose:** To assess the impact of spin-orbit currents on the electromagnetic- and weak-charge radii of a variety of nuclei. Special emphasis is placed on the experimentally accessible electroweak skin, defined as the difference between weak-charge and electromagnetic-charge radii. **Methods:** Two accurately calibrated relativistic mean field models are used to compute proton, neutron, charge, and weak-charge radii of a variety of nuclei. **Results:** We find that spin-orbit contributions to the electroweak skin of light neutron-rich nuclei, such as ^{22}O and ^{48}Ca, are significant and result in a substantial increase in the size of the electroweak skin relative to the neutron skin. **Conclusions:** Given that spin-orbit contributions to both the charge and weak-charge radii of nuclei are often as large as present or anticipated experimental error bars, future calculations must incorporate spin-orbit currents in the calculation of electroweak form factors.

PACS numbers: 21.10.Gv, 25.30.Bf, 24.80.+y,

I. INTRODUCTION

Recently the *Lead Radius EXperiment* ("PREX") at the Jefferson Laboratory used parity violating electron scattering to probe the weak-charge density of ^{208}Pb [1, 2]. In Born approximation, the parity violating asymmetry—the fractional difference in cross sections for positive and negative helicity electrons—is directly proportional to the weak form factor, which is the Fourier transform of the weak-charge density. Although for a heavy nucleus one must include the effects of Coulomb distortions, these have been accurately calculated [3, 4]. Thus, parity-violating electron scattering can be used with as much confidence to measure the weak-charge form factor of the nucleus as conventional electron scattering has been used throughout the years to accurately map the electromagnetic charge distribution. Many details of a practical parity-violating experiment, along with a number of theoretical corrections, have been discussed in Ref. [5]. PREX demonstrated excellent control of systematic errors and showed that accurate and model independent measurements of weak-charge densities are now feasible.

In this paper we focus on the *electroweak skin* of a nucleus which we define as

$$R_{\text{wskin}} \equiv R_{\text{wk}} - R_{\text{ch}} \,, \tag{1}$$

where R_{wk} and R_{ch} are the root-mean-square radii of the weak-charge and electromagnetic-charge densities, respectively, Note that unlike the point-neutron and point-proton densities, the weak-charge density—the source for the Z^0 weak boson—and the electromagnetic-charge density are physical observables. For simplicity, we refer to R_{wskin} as the *weak skin*. Given that the charge radius of ^{208}Pb is very accurately known [6], the determination of the weak form factor of ^{208}Pb by the PREX collaboration resulted in the following value for its weak skin [2]:

$$R_{\text{wskin}}(^{208}\text{Pb}) = 0.32 \pm 0.18(\text{exp}) \pm 0.03(\text{mod}) \,\text{fm} \,. \tag{2}$$

Note that the experimental error ("exp") includes both statistical and systematic errors while the small model error ("mod") describes the sensitivity in the extraction of R_{wk} due to uncertainties in the surface thickness [2]. Although the statistical accuracy of the measurement was compromised by unforeseen technical difficulties, a follow-up measurement ("PREX-II") designed to achieve the original ± 0.05 fm goal has been proposed and accepted [7]. Moreover, a fresh

---

*Electronic address: horowit@indiana.edu
†Electronic address: jpiekarewicz@fsu.edu

new proposal has been made to use parity-violating electron scattering to measure the weak form factor of ^{48}Ca at a momentum transfer of $q = 0.778\,\text{fm}^{-1}$. The *Calcium Radius EXperiment* ("C-REX") is designed to constrain the weak-charge radius of ^{48}Ca to an accuracy of $\pm 0.03\,\text{fm}$ [8]. A measurement in a smaller neutron-rich nucleus is desirable because the form factor can be measured at a larger momentum transfer where the parity-violating asymmetry is larger; for comparison, the weak form factor in ^{208}Pb was measured at $q = 0.475\,\text{fm}^{-1}$. In addition, a precise measurement of the weak radius of ^{48}Ca may have a significant impact on nuclear structure as it provides information that is independent and complementary to that found in ^{208}Pb [9]. Furthermore, it is reasonable to expect first-principle calculations of the structure of ^{48}Ca where the role of 3-neutron forces may be particularly interesting and important. Finally, in conjunction with PREX and PREX-II, C-REX will provide vital guidance in areas as diverse as atomic parity violation [10, 11], heavy-ion collisions [12–16], and neutron-star structure [17–22]. Given the expected accuracy of these pioneering experiments, it is critical to assess the role of *"sub-leading"* contributions to the weak skin of these nuclei. Thus, it is the main goal of the present contribution to quantify the impact of spin-orbit currents on the electroweak skin of a variety of nuclei. We note that meson-exchange currents—which are not considered in this contribution—can change the distribution of both electromagnetic and weak charge. For example $\rho\pi\gamma$ and $\omega\sigma\gamma$ meson-exchange currents (MEC) are known to modify significantly the electromagnetic form factors of the deuteron [23]. However, heavy mesons are unlikely to transport charge over large distances, so we do not expect significant MEC corrections to either R_{ch} or R_{wk} for a heavy nucleus. Yet MEC corrections could be more important for the case of the weak skin ($R_{\text{wk}} - R_{\text{ch}}$) and this deserves further consideration.

The result depicted in Eq. (2) represents a true experimental milestone. It provides direct experimental evidence that the weak-charge density in ^{208}Pb extends further out than the corresponding electromagnetic-charge density. That is, there is an enhancement of weak charges (which are dominated by neutrons) relative to electromagnetic charges (which are dominated by protons) near the nuclear surface. A quantity that is closely related to the weak skin of a heavy nucleus is the *neutron skin*. In analogy to the weak skin, the neutron skin is defined as the difference between the point neutron R_n and point proton R_p root-mean-square radii:

$$R_{\text{nskin}} \equiv R_n - R_p \ . \tag{3}$$

The weak and neutron skins are closely related to each other because the weak charge of a neutron (≈ -1) is much larger than the weak charge of the proton (≈ 0.07) largely in the same way as the electromagnetic charge of the proton is much larger than that of the neutron. Indeed, to a good approximation the weak form factor of a single nucleon equals the negative of the electromagnetic form factor of its isospin partner (see Appendix). The structure of a nucleus is often modeled in terms of point nucleons interacting via strong nuclear potentials or meson exchanges. Therefore, nuclear-structure calculations provide predictions for the neutron skin whereas it is the weak skin that is experimentally accesible. In the present paper we calculate the difference between R_{wskin} and R_{nskin} that originates from the internal structure of the nucleon. The internal structure of the nucleon is contained in a variety of well-measured single nucleon electromagnetic and weak form factors. The electromagnetic size of the nucleon leads to a charge radius of the nucleus R_{ch} that is slightly larger than the point proton radius R_p due (mostly) to the charge radius of a single proton r_p ($R_{\text{ch}}^2 \approx R_p^2 + r_p^2$). Similarly, the weak radius R_{wk} is slightly larger than R_n (mostly) because of the weak-charge radius of a single neutron. Note that we have reserved the use of upper-case R to nuclear radii and of lower-case r to the radii of single nucleons.

The manuscript has been organized as follows. In Sec. II we outline the formalism used to calculate weak and electromagnetic charge form factors and densities. These form factors are computed from one-body currents that include weak and electromagnetic single-nucleon form factors. We discuss in detail the contribution to both of the form factors from the spin-orbit currents. For a recent reference on the impact of spin-orbit currents on the charge density of light nuclei see Ref. [24]. However, to our knowledge the role of spin-orbit currents on the weak-charge density has never been studied. In Sec. III we present results for proton, neutron, charge, and weak radii for a variety of nuclei. Spin-orbit corrections are particularly large for light nuclei and we observe a significant increase in the weak skin of these nuclei relative to their neutron skin. We offer our conclusion in Sec. IV.

II. FORMALISM

We start the formalism by writing the most general form of the single-nucleon matrix elements of the electroweak current consistent with Lorentz covariance and parity invariance. That is [25],

$$\langle N(\mathbf{p}',s')|\hat{J}_{\text{EM}}^{\mu}|N(\mathbf{p},s)\rangle = \overline{U}(\mathbf{p}',s')\left[F_1\gamma^{\mu} + iF_2\sigma^{\mu\nu}\frac{q_\nu}{2M}\right]U(\mathbf{p},s) \ , \tag{4a}$$

$$\langle N(\mathbf{p}',s')|\hat{J}_{\text{NC}}^{\mu}|N(\mathbf{p},s)\rangle = \overline{U}(\mathbf{p}',s')\left[\widetilde{F}_1\gamma^{\mu} + i\widetilde{F}_2\sigma^{\mu\nu}\frac{q_\nu}{2M}\right]U(\mathbf{p},s) \ , \tag{4b}$$

where $U(\mathbf{p},s)$ are on-shell nucleon spinors, $q \equiv p' - p$ is the four momentum transfer to the nucleon, and $F_{1,2}(\widetilde{F}_{1.2})$ are electromagnetic (weak-neutral vector) Dirac and Pauli form factors, respectively. Note that the axial-vector component of the weak neutral current makes no contribution to the elastic form factor of a nuclear ground state of definite parity. As can be seen from the above equations, the formal structure of the vector current is the same regardless of whether one considers electromagnetic or weak matrix elements or whether one considers protons or neutrons. Thus, for illustration purposes we focus the derivation on the proton contribution to the charge form factor.

A. Charge Form Factor

Throughout this contribution we will assume the validity of the impulse approximation, namely, that the single-nucleon form factors defined in Eq. (4) may be used without modification in the nuclear medium. Moreover, we rely on an alternative description of the single-nucleon electromagnetic current based on the electric and magnetic Sachs form factors rather than on $F_{1,2}$. The two sets of form factors are related as follows:

$$G_{\mathrm{E}}(Q^2) \equiv F_1(Q^2) - \tau F_2(Q^2) \,, \tag{5a}$$
$$G_{\mathrm{M}}(Q^2) \equiv F_1(Q^2) + F_2(Q^2) \,, \tag{5b}$$

where $Q^2 = -q_\mu q^\mu > 0$ and $\tau = Q^2/4M^2$. In turn, the electromagnetic current operator may be written as

$$\hat{J}^\mu_{\mathrm{EM}} = G_{\mathrm{E}}\gamma^\mu + \left(\frac{G_{\mathrm{M}} - G_{\mathrm{E}}}{1 + \tau}\right)\left[\tau\gamma^\mu + i\sigma^{\mu\nu}\frac{q_\nu}{2M}\right] \,. \tag{6}$$

Given that we are interested in computing the elastic form factor of spherical nuclei, only the density (*i.e.*, the zeroth component of the current) needs to be consider. Such density is given by

$$\hat{J}^0_{\mathrm{EM}} \equiv \rho_{\mathrm{EM}} = G_{\mathrm{E}}\gamma^0 + \left(\frac{G_{\mathrm{M}} - G_{\mathrm{E}}}{1 + \tau}\right)\left[\tau\gamma^0 + \gamma^0\frac{\boldsymbol{\gamma} \cdot \mathbf{q}}{2M}\right] \,. \tag{7}$$

Thus, in the impulse approximation, the charge form factor of the nucleus may written as follows:

$$ZF_{\mathrm{ch}}(q) = G_{\mathrm{E}}(q^2)F_{\mathrm{V}}(q) + \left(\frac{G_{\mathrm{M}}(q^2) - G_{\mathrm{E}}(q^2)}{1 + \tau}\right)\left[\tau F_{\mathrm{V}}(q) + \frac{q}{2M}F_{\mathrm{T}}(q)\right] \,, \tag{8}$$

where Z is the number of protons and the charge form factor of the nucleus has been normalized to $F_{\mathrm{ch}}(q = 0) = 1$. Note that all nuclear structure information is contained in the elastic (point-nucleon) vector and tensor form factors defined as

$$F_{\mathrm{V}}(q) = \int \bar{\psi}(\mathbf{r})e^{i\mathbf{q}\cdot\mathbf{r}}\gamma^0\psi(\mathbf{r})d^3r \,, \tag{9a}$$

$$F_{\mathrm{T}}(q) = \int \bar{\psi}(\mathbf{r})e^{i\mathbf{q}\cdot\mathbf{r}}\gamma^0\boldsymbol{\gamma} \cdot \hat{\mathbf{q}}\,\psi(\mathbf{r})d^3r \,. \tag{9b}$$

We now proceed to evaluate these two nuclear form factors using a relativistic mean-field approximation.

B. Relativistic Mean-Field Approximation

In a relativistic mean-field approximation, the eigenstates of the Dirac equation corresponding to a spherically symmetric ground state may be classified according to a generalized angular momentum κ [26]. That is, the single-particle solutions of the Dirac equation may be written as

$$\mathcal{U}_{n\kappa m}(\mathbf{r}) = \frac{1}{r}\begin{pmatrix} g_{n\kappa}(r)\mathcal{Y}_{+\kappa m}(\hat{\mathbf{r}}) \\ if_{n\kappa}(r)\mathcal{Y}_{-\kappa m}(\hat{\mathbf{r}}) \end{pmatrix} \,, \tag{10}$$

where n and m are the principal and magnetic quantum numbers, respectively, and the spin-spherical harmonics are defined as follows:

$$\mathcal{Y}_{\kappa m}(\hat{\mathbf{r}}) \equiv \langle \hat{\mathbf{r}}|l\tfrac{1}{2}jm\rangle \,; \quad j = |\kappa| - \frac{1}{2} \,; \quad l = \begin{cases} \kappa \,, & \text{if } \kappa > 0; \\ -1 - \kappa \,, & \text{if } \kappa < 0. \end{cases} \tag{11}$$

Note that for the phase convention adopted in Eq. (10) (namely, the relative factor of i) both $g(r)$ and $f(r)$ are real functions in the case of real mean-field potentials. Further, the following spinor normalization has been used:

$$\int \mathcal{U}_{n\kappa m}^\dagger(\mathbf{r})\mathcal{U}_{n\kappa m}(\mathbf{r})d^3r = \int_0^\infty \left[g_{n\kappa}^2(r) + f_{n\kappa}^2(r)\right]dr = 1\,. \tag{12}$$

Thus, in a mean-field approximation the vector and tensor form factors may be expressed as a sum over occupied single-particle states. That is,

$$F_\text{V}(q) = \sum_{n\kappa m}\int \overline{\mathcal{U}}_{n\kappa m}(\mathbf{r})j_0(qr)\gamma^0\,\mathcal{U}_{n\kappa m}(\mathbf{r})d^3r\,, \tag{13a}$$

$$F_\text{T}(q) = \sum_{n\kappa m}\int \overline{\mathcal{U}}_{n\kappa m}(\mathbf{r})j_1(qr)\,i\gamma^0\boldsymbol{\gamma}\cdot\hat{\mathbf{r}}\,\mathcal{U}_{n\kappa m}(\mathbf{r})d^3r\,. \tag{13b}$$

Here $j_l(qr)$ are spherical Bessel functions and the sum over single-particle quantum numbers $\{n\kappa m\}$ is restricted to the occupied orbitals. Note that by virtue of the spherical symmetry of the nuclear form factors, all explicit dependence on $\hat{\mathbf{q}}$ has been eliminated through an "angle-average" (i.e., by integrating over $d\hat{\mathbf{q}}/4\pi$). This fact leads to a considerable simplification and enables one to readily perform the integrals over the remaining solid angle. One finally obtains:

$$F_\text{V}(q) = \sum_{n\kappa}(2j+1)\int_0^\infty \left[g_{n\kappa}^2(r) + f_{n\kappa}^2(r)\right]j_0(qr)dr\,, \tag{14a}$$

$$F_\text{T}(q) = \sum_{n\kappa}2(2j+1)\int_0^\infty g_{n\kappa}(r)f_{n\kappa}(r)j_1(qr)dr\,. \tag{14b}$$

Note that for a spherically symmetric ground state there is a third independent "scalar" form factor that is identical to the vector one except for a relative minus sign between upper and lower components. Given the form of the electromagnetic current adopted in Eq. (4), and ignoring possible off-shell ambiguities, the scalar form factor plays no role in the present discussion.

In summary, nuclear charge and weak form factors—both normalized to one at $q=0$—are now obtained from Eq. (8) by properly adding proton and neutron contributions. That is,

$$ZF_\text{ch}(q) = \sum_{i=p,n}\left(G_\text{E}^i(q^2)F_\text{V}^i(q) + \left(\frac{G_\text{M}^i(q^2)-G_\text{E}^i(q^2)}{1+\tau}\right)\left[\tau F_\text{V}^i(q) + \frac{q}{2M}F_\text{T}^i(q)\right]\right)\,, \tag{15a}$$

$$Q_\text{wk}F_\text{wk}(q) = \sum_{i=p,n}\left(\widetilde{G}_\text{E}^i(q^2)F_\text{V}^i(q) + \left(\frac{\widetilde{G}_\text{M}^i(q^2)-\widetilde{G}_\text{E}^i(q^2)}{1+\tau}\right)\left[\tau F_\text{V}^i(q) + \frac{q}{2M}F_\text{T}^i(q)\right]\right)\,, \tag{15b}$$

where Q_wk is the weak-vector charge of the nucleus (see Appendix).

C.   Electromagnetic and Weak Charge Radii

The experimentally measurable electromagnetic R_ch and weak R_wk charge radii are obtained from the slope of the respective form factors at the origin. That is,

$$R_\text{ch} = -6\frac{dF_\text{ch}}{dq^2}\bigg|_{q=0} \quad\text{and}\quad R_\text{wk} = -6\frac{dF_\text{wk}}{dq^2}\bigg|_{q=0}\,. \tag{16}$$

Although in the next section we provide results in the form of tables and figures, it is illuminating to discuss the particle content of both R_ch and R_wk. We start with the former. According to Eq. (15a), the electromagnetic charge form factor to first order in q^2 may be written as follows:

$$ZF_\text{ch}(q) = Z\left(1 - \frac{q^2}{6}R_p^2\right)\left(1 - \frac{q^2}{6}r_p^2\right) + \frac{q^2}{4M^2}\kappa_p Z(1 + f_\text{T}^p) + \dots$$

$$+ N\left(1 - \frac{q^2}{6}R_n^2\right)\left(0 - \frac{q^2}{6}r_n^2\right) + \frac{q^2}{4M^2}\kappa_n N(1 + f_\text{T}^n) + \dots \tag{17}$$

where $r_{p,n}^2$ and $\kappa_{p,n}$ are single-nucleon electromagnetic mean-square radii and anomalous magnetic moments, respectively. Note that we have defined

$$f_{\mathrm{T}}^p = \frac{4M}{3Z} \sum_{n\kappa} (2j+1) \int_0^\infty r g_{n\kappa}^p(r) f_{n\kappa}^p(r) dr \,, \tag{18a}$$

$$f_{\mathrm{T}}^n = \frac{4M}{3N} \sum_{n\kappa} (2j+1) \int_0^\infty r g_{n\kappa}^n(r) f_{n\kappa}^n(r) dr \,. \tag{18b}$$

Using Eq. (17) one can readily obtained an expression for the electromagnetic charge radius of the nucleus. That is,

$$R_{\mathrm{ch}}^2 = R_p^2 + r_p^2 + \langle r_p^2 \rangle_{\mathrm{so}} + \frac{N}{Z} \left(r_n^2 + \langle r_n^2 \rangle_{\mathrm{so}} \right) \,, \tag{19}$$

where "spin-orbit" contributions to the charge radius have been defined as follows:

$$\langle r_p^2 \rangle_{\mathrm{so}} = -\frac{3\kappa_p}{2M^2} (1 + f_{\mathrm{T}}^p) \,, \tag{20a}$$

$$\langle r_n^2 \rangle_{\mathrm{so}} = -\frac{3\kappa_n}{2M^2} (1 + f_{\mathrm{T}}^n) \,. \tag{20b}$$

In the context of a relativistic mean-field approximation—where both upper and lower components are self-consistently generated from the Hartree equations—there are no further simplifications. However, one can shed light into the nature of the spin-orbit contribution by generating the lower component from the upper component by assuming a free-space relation. That is,

$$f_{n\kappa}(r) = \frac{1}{2M} \left(\frac{d}{dr} + \frac{\kappa}{r} \right) g_{n\kappa}(r) \,. \tag{21}$$

In this free-space limit an enormous simplification ensues, as the tensor integrals given in Eq. (18) can be evaluated in closed form. In this limit the spin-orbit contributions to the charge radius become

$$\langle r_p^2 \rangle_{\mathrm{so}} = -\frac{3\kappa_p}{2M^2}(1 + f_{\mathrm{T}}^p) \rightarrow -\frac{2\kappa_p}{M^2 Z} \sum_{n\kappa} \mathrm{sgn}(\kappa) l(l+1) \,, \tag{22a}$$

$$\langle r_n^2 \rangle_{\mathrm{so}} = -\frac{3\kappa_n}{2M^2}(1 + f_{\mathrm{T}}^n) \rightarrow -\frac{2\kappa_n}{M^2 N} \sum_{n\kappa} \mathrm{sgn}(\kappa) l(l+1) \,. \tag{22b}$$

The above results indicate that: (a) there is no contribution from s-states and (b) there is an exact cancellation between spin-orbit partners, which have the same l but opposite signs for κ. Thus, in the particular case of ^{48}Ca the only spin-orbit contribution comes from the "unpaired" $1f_{7/2}$ neutron orbital. For this case we obtain the following figure of merit:

$$\langle r^2 \rangle_{\mathrm{so}} \equiv \frac{N}{Z} \langle r_n^2 \rangle_{\mathrm{so}} = \frac{6\kappa_n}{5M^2} \approx -0.101 \,\mathrm{fm}^2 \,. \tag{23}$$

Thus, the spin-orbit contribution amounts to approximately -0.015 fm of the total charge radius of ^{48}Ca, which is significantly larger than the quoted experimental error [6]. Note that in a self-consistent RMF approximation the cancellation between spin-orbit partners, although still large, will be incomplete. However, there is an additional cancellation between neutron and proton orbitals with the same quantum numbers due to their almost equal but opposite anomalous magnetic moments. Ultimately, the spin-orbit contribution is dominated by the unpaired orbitals.

To obtain the weak-charge radius R_{wk} one proceeds in an analogous manner but now starting from Eq. (15b). Expanding the weak charge form factor to first order in q^2 one obtains

$$Q_{\mathrm{wk}} F_{\mathrm{wk}}(q) = Z \left(1 - \frac{q^2}{6} R_p^2 \right) g_{\mathrm{v}}^{\mathrm{p}} \left(1 - \frac{q^2}{6} \tilde{r}_p^2 \right) + \frac{q^2}{4M^2} \tilde{\kappa}_p Z (1 + f_{\mathrm{T}}^p) + \dots$$

$$+ N \left(1 - \frac{q^2}{6} R_n^2 \right) g_{\mathrm{v}}^{\mathrm{n}} \left(1 - \frac{q^2}{6} \tilde{r}_n^2 \right) + \frac{q^2}{4M^2} \tilde{\kappa}_n N (1 + f_{\mathrm{T}}^n) + \dots \tag{24}$$

where $g_{\mathrm{v}}^{\mathrm{p}} = 0.0721$ and $g_{\mathrm{v}}^{\mathrm{n}} = -0.9878$ are (radiatively-corrected) single-nucleon weak-vector charges [2, 25]. Note that the weak-charge radii $\tilde{r}_{p,n}^2$ and anomalous weak-magnetic moments $\tilde{\kappa}_{p,n}$ may be expressed exclusively in terms

of the corresponding electromagnetic and strange-quark quantities, as indicated in the Appendix. In this way, the weak-charge radius of the nucleus can now be readily extracted from Eq. (24). That is,

$$R_{\rm wk}^2 = \frac{Z}{Q_{\rm wk}} \left[g_{\rm v}^{\rm p} \left(R_p^2 + \tilde{r}_p^2 \right) + \langle \tilde{r}_p^2 \rangle_{\rm so} \right] + \frac{N}{Q_{\rm wk}} \left[g_{\rm v}^{\rm n} \left(R_n^2 + \tilde{r}_n^2 \right) + \langle \tilde{r}_n^2 \rangle_{\rm so} \right] \tag{25}$$

where spin-orbit contributions to the weak-charge radius are defined in analogy to Eq. (22):

$$\langle \tilde{r}_p^2 \rangle_{\rm so} = -\frac{3\widetilde{\kappa}_p}{2M^2} \left(1 + f_{\rm T}^p \right), \tag{26a}$$

$$\langle \tilde{r}_n^2 \rangle_{\rm so} = -\frac{3\widetilde{\kappa}_n}{2M^2} \left(1 + f_{\rm T}^n \right). \tag{26b}$$

Given that $Q_{\rm wk} = Z g_{\rm v}^{\rm p} + N g_{\rm v}^{\rm n}$ (with $g_{\rm v}^{\rm p} \approx 0$ and $g_{\rm v}^{\rm n} \approx -1$) the weak-charge radius of the nucleus $R_{\rm wk}$ is dominated by the contribution from the neutron radius R_n.

We close this section by providing a figure of merit for the weak-charge radius of ^{48}Ca by neglecting the strange-quark contribution and by assuming the free-space relation in the evaluation of the tensor integrals [Eq. (18)]. We obtain:

$$R_{\rm wk}^2 = \frac{Z}{Q_{\rm wk}} \left[g_{\rm v}^{\rm p} R_p^2 + g_{\rm v}^{\rm p} r_p^2 + g_{\rm v}^{\rm n} r_n^2 \right] + \frac{N}{Q_{\rm wk}} \left[g_{\rm v}^{\rm n} R_n^2 + g_{\rm v}^{\rm n} r_p^2 + g_{\rm v}^{\rm p} r_n^2 + \frac{6}{7M^2} \left(g_{\rm v}^{\rm n} \kappa_p + g_{\rm v}^{\rm p} \kappa_n \right) \right]. \tag{27}$$

Note that in the above expression single-nucleon mean-square radii ($r_{p,n}^2$) as well as anomalous magnetic moments ($\kappa_{p,n}$) are purely electromagnetic. Assuming (point) proton and neutron radii for ^{48}Ca as predicted by the FSUGold model [27] (or "FSU" for short) we obtain

$$R_{\rm wk} = 3.679(3.669)\,{\rm fm}, \tag{28}$$

where the quantity in parenthesis represents the FSU prediction without including the spin-orbit contribution that amounts to:

$$\langle \tilde{r}^2 \rangle_{\rm so} \equiv \frac{N}{Q_{\rm wk}} \langle \tilde{r}_n^2 \rangle_{\rm so} = \frac{N}{Q_{\rm wk}} \frac{6(g_{\rm v}^{\rm n} \kappa_p + g_{\rm v}^{\rm p} \kappa_n)}{7M^2} \approx +0.077\,{\rm fm}^2. \tag{29}$$

Given that the weak spin-orbit contribution has the opposite sign as the corresponding electromagnetic one [see Eq. (23)], the spin-orbit contribution to the weak skin of ^{48}Ca is significant; of about 0.03 fm (see Table II). This is within the projected accuracy of the proposed C-REX experiment [8].

D. Electroweak Nucleon Form Factors

Since our main objective is the calculation of electromagnetic- and weak-charge radii, we adopt a simple dipole parametrization of the single nucleon form factors that is accurate at moderate values of the momentum transfer. That is, we define electromagnetic single nucleon form factors as follows [28]:

$$G_{\rm E}^p(Q^2) = \frac{G_{\rm M}^p(Q^2)}{\mu_p} = \frac{G_{\rm M}^n(Q^2)}{\mu_n} = G_{\rm D}(Q^2), \tag{30}$$

where the dipole form factor is given by

$$G_{\rm D}(Q^2) = \left(1 + \frac{Q^2}{12} r_p^2 \right)^{-2}. \tag{31}$$

Here $r_p^2 = 0.769\,{\rm fm}^2$ is the mean-square proton radius, $\mu_p = 2.793$ the proton magnetic moment, and $\mu_n = -1.913$ the neutron magnetic moment. For the electromagnetic neutron form factor—which vanishes at $Q^2 = 0$—we rely on the following Galster parametrization [28]:

$$G_{\rm E}^n(Q^2) = -\left(\frac{Q^2 r_n^2/6}{1 + Q^2/M^2} \right) G_{\rm D}(Q^2), \tag{32}$$

where $r_n^2 = -0.116 \, \text{fm}^2$ is the electromagnetic mean-square radius of the neutron. Note that all form factors are expressed exclusively in terms of experimentally determined single nucleon mean-square radii and magnetic moments [29]. Finally, given that the strange-quark form factors of the nucleon are small at small momentum transfers, we will ignore them in this contribution. In this case, the weak-charge form factors of the nucleon can be expressed exclusively in terms of the corresponding electromagnetic form factors given here and the weak charges of the nucleon (see Appendix). For example, using Eqs. (A.8) and (A.9) the weak mean-square radii and magnetic moments are given by

$$\tilde{r}_p^2 = 2.358 \, \text{fm}^2 \,, \quad \tilde{\mu}_p = +2.091 \,; \tag{33a}$$

$$\tilde{r}_n^2 = 0.777 \, \text{fm}^2 \,, \quad \tilde{\mu}_n = -2.897 \,. \tag{33b}$$

III. RESULTS

In this section we present results—primarily proton, neutron, charge, and weak-charge radii—for a variety of nuclei as predicted by two accurately calibrated relativistic mean field models: FSU [27] and NL3 [30, 31]. We start by displaying in Table I the contribution from the individual single-particle orbitals in ^{48}Ca to the charge and weak-charge spin-orbit radius. For illustration purposes, the predictions have been made using only the FSU parametrization. The quantities in parenthesis represent the results obtained by assuming a free-space relation between upper and lower components, as indicated in Eq. (21). Qualitatively, all major trends in the results may be understood using this simplified case. In particular, the results displayed in parenthesis in Table I: (i) are independent of the dynamics, (ii) scale as $l(l+1)$, and (iii) display an exact cancellation among spin-orbit partners [see Eqs. (22)]. Thus, in this limit the sole contribution to the spin-orbit radius comes from unpaired spin-orbit partners (an unpaired $1f_{7/2}$ neutron orbital in the case of ^{48}Ca). Given the natural ordering of spin-orbit partners in nuclei, namely, the $\kappa < 0$ orbital more deeply bound than the $\kappa > 0$ orbital, the spin-orbit contribution to the charge radius is always negative in the case of unpaired neutrons. Note that the situation is reversed in the case of protons due to an anomalous magnetic moment of opposite sign to that of the neutron. Moreover, in the case of the weak-charge radius, the spin-orbit contribution is always of opposite sign—for both neutrons and protons—than in the electromagnetic case. Indeed, for a given nucleon orbital the ratio of spin-orbit contributions is given by the following simple expression:

$$\frac{\langle \tilde{r}_{p,n}^2 \rangle_{\text{so}}}{\langle r_{p,n}^2 \rangle_{\text{so}}} = \left(\frac{\widetilde{\kappa}_{p,n}}{\kappa_{p,n}} \right) \left(\frac{Z}{Q_{\text{wk}}} \right) \approx \left(\frac{\kappa_{n,p}}{\kappa_{p,n}} \right) \left(\frac{Z}{N} \right) < 0 \,. \tag{34}$$

Hence, although in general small, charge and weak-charge spin-orbit radii contribute with the same sign to the weak skin of a nucleus. For example, as indicated in Table II the spin-orbit contribution amounts to about 0.04 fm in the case of the weak skin of ^{22}O and to about 0.03 fm for ^{48}Ca.

Also shown in Table I are predictions from the self-consistent RMF approach, where now both upper and lower components are dynamically generated. The qualitative trends discussed previously are clearly preserved, although now the cancellation among spin-orbit partners is incomplete. For example, the contributions from the 1p orbitals differ from each other by about 55-60%. However, although the spin-orbit cancellation is incomplete, there is an additional cancellation stemming from the nucleon anomalous magnetic moments (which are nearly equal in magnitude but opposite in sign). Ultimately, the spin-orbit radius continues to be dominated by the unpaired $1f_{7/2}$ neutron orbital. Note, however, that the exact RMF prediction exceeds by about 30% the analytic result obtained from assuming the free-space relation. This enhancement is due to the reduction of the effective nucleon mass in the nuclear medium.

In Table II predictions are displayed for the root-mean-square radii for a variety of magic (or semi-magic) nuclei as predicted by the NL3 and FSU models. Also shown (last three entries) are nuclei of relevance to the atomic-parity violating program [11]. These nuclei are relevant as they are members of long chains of naturally occurring isotopes that help eliminate uncertainties in the atomic theory by forming suitable ratios of parity-violating observables. By doing so, uncertainties in neutron radii become the limiting factor in the search of physics beyond the standard model. Note that the NL3 and FSU models—although both accurately calibrated—predict large differences in neutron radii. However, we caution the reader that in the case of semi-magic and open-shell nuclei, such as ^{118}Sn, ^{138}Ba, ^{158}Dy, and ^{176}Yb, nuclear deformation and pairing correlations—which have not been included—may play an important role. Moreover, although accurately calibrated, note that most mean-field models (including the ones used here) are

$nlj\,(\kappa)$	$\langle r_p^2 \rangle_{\mathrm{so}}$	$\langle r_n^2 \rangle_{\mathrm{so}}$	$\langle r^2 \rangle_{\mathrm{so}}$
$1\mathrm{s}_{1/2}\,(-1)$	$+0.570(+0.000)$	$-0.648(+0.000)$	$-0.078(+0.000)$
$1\mathrm{p}_{3/2}\,(-2)$	$+3.107(+1.583)$	$-3.409(-1.690)$	$-0.302(-0.107)$
$1\mathrm{p}_{1/2}\,(+1)$	$-1.997(-1.583)$	$+2.113(+1.690)$	$+0.116(+0.107)$
$1\mathrm{d}_{5/2}\,(-3)$	$+7.138(+4.750)$	$-7.710(-5.069)$	$-0.572(-0.319)$
$1\mathrm{d}_{3/2}\,(+2)$	$-6.205(-4.750)$	$+6.613(+5.069)$	$+0.408(+0.319)$
$2\mathrm{s}_{1/2}\,(-1)$	$+0.178(+0.000)$	$-0.177(+0.000)$	$+0.001(+0.000)$
$1\mathrm{f}_{7/2}\,(-4)$	$+0.000(+0.000)$	$-13.042(-10.138)$	$-13.042(-10.138)$
Total	$+2.791(+0.000)$	$-16.260(-10.138)$	$-13.469(-10.138)$
$nlj\,(\kappa)$	$\langle \tilde{r}_p^2 \rangle_{\mathrm{so}}$	$\langle \tilde{r}_n^2 \rangle_{\mathrm{so}}$	$\langle \tilde{r}^2 \rangle_{\mathrm{so}}$
$1\mathrm{s}_{1/2}\,(-1)$	$-0.489(+0.000)$	$+0.494(+0.000)$	$+0.005(+0.000)$
$1\mathrm{p}_{3/2}\,(-2)$	$-2.669(-1.360)$	$+2.595(+1.286)$	$-0.074(-0.074)$
$1\mathrm{p}_{1/2}\,(+1)$	$+1.716(+1.360)$	$-1.608(-1.286)$	$+0.108(+0.074)$
$1\mathrm{d}_{5/2}\,(-3)$	$-6.132(-4.081)$	$+5.869(+3.859)$	$-0.263(-0.222)$
$1\mathrm{d}_{3/2}\,(+2)$	$+5.331(+4.081)$	$-5.034(-3.859)$	$+0.297(+0.222)$
$2\mathrm{s}_{1/2}\,(-1)$	$-0.153(+0.000)$	$+0.135(+0.000)$	$-0.018(+0.000)$
$1\mathrm{f}_{7/2}\,(-4)$	$+0.000(+0.000)$	$+9.928(+7.717)$	$+9.928(+7.717)$
Total	$-2.396(+0.000)$	$+12.379(+7.717)$	$+9.983(+7.717)$

TABLE I: Contributions from the individual single-particle orbitals to the spin-orbit component of the mean square charge radius (upper table) and weak-charge radius (lower table) of ^{48}Ca. Mean square radii are expressed in units of $10^{-2}\,\mathrm{fm}^2$ and were generated using the FSU interaction. Quantities displayed in parenthesis have been computed using the free-space relation given in Eq. (21).

unable to predict with high accuracy charge radii throughout the nuclear chart. Indeed, sometimes even trends along an isotopic chain are difficult to reproduce; particularly noteworthy is the case of ^{40}Ca and ^{48}Ca, where the charge radius of the former exceeds (slightly) the one of the latter [6].

The first three columns of numbers in Table II provide predictions for the point-proton, point-neutron, and charge radii of several nuclei. To a large extent these results are expected and in some particular cases (such as ^{208}Pb) have been extensively discussed. For example, given that the charge form factor of many of these nuclei has been accurately measured via (parity conserving) elastic electron scattering, this information—mostly in the form of charge radii—has been incorporated into the calibration of the RMF models. Thus, the predictions of both models for charge radii are in fairly good agreement (*e.g.*, they differ by only 0.009 fm in the case of ^{208}Pb). In contrast, the lack of reliable neutron form factors leaves the isovector sector of the relativistic functionals largely unconstrained, thereby generating large differences in the predictions of neutron radii (*e.g.*, 0.064 fm, or more than 1%, in the case of ^{208}Pb). Fortunately, the prospects of constraining the isovector sector through the measurement of neutron-radii are very good. Indeed, the vigorous and highly successful parity-violating program at JLAB has recently provided the first model-independence evidence in favor of a weak skin in ^{208}Pb. Moreover, a follow-up measurement has been approved to achieve the original ± 0.05 fm goal (PREX-II) and a fresh new one (C-REX) has been proposed to constrain the neutron radius of ^{48}Ca to ± 0.03 fm. It is therefore critical and timely to assess the impact of the spin-orbit corrections on the weak radius of these nuclei—which until now has never been considered.

Given the enormous cancellation among spin-orbit partners and proton-neutron orbitals with the same quantum numbers, the spin-orbit contribution to the charge and weak-charge radii lacks the coherence displayed by the dominant vector form factor [see Eqs. (14)]. Thus, one expects that the spin-orbit correction will be largest for light nuclei with unpaired spin-orbit partners. Indeed, Table II displays relatively large spin-orbit contributions—of ≈ 0.045 fm and ≈ 0.03 fm—to the weak skin of ^{22}O and ^{48}Ca, respectively. These spin-orbit corrections are commensurate with the projected experimental uncertainty so they must be included in the prediction of both charge and weak-charge radii. Charge and weak-charge densities for ^{22}O and ^{48}Ca—with and without spin-orbit corrections—as predicted by the FSU interaction are also shown in Fig. 1. Note that the effect from neglecting the spin-orbit contribution is clearly discernible in the figure, as is the fact that the modification to the charge and weak-charge radii goes in the opposite direction—thereby enhancing its contribution to the weak skin. As alluded earlier, the impact of the spin-orbit contribution diminishes with increasing baryon number and amounts to only ≈ 0.002 fm in the case of the weak radius of ^{208}Pb—significantly below the anticipated ± 0.05 fm of the PREX-II measurement. Yet, the ≈ 0.004 fm contribution to the charge radius of ^{208}Pb is significantly larger than the minute 0.0009 fm error quoted in Ref. [6]. In the particular case of atomic nuclei of relevance to the atomic parity violating program, the spin-orbit contribution to

Nucleus	Model	R_p	R_n	R_{ch}	R_{wk}	R_{nskin}	R_{wskin}
^{22}O	NL3	2.593	3.026	2.671(2.700)	3.172(3.158)	0.433	0.502(0.458)
	FSU	2.580	2.997	2.658(2.688)	3.144(3.129)	0.417	0.487(0.442)
^{48}Ca	NL3	3.379	3.605	3.449(3.467)	3.724(3.711)	0.226	0.275(0.243)
	FSU	3.366	3.563	3.435(3.455)	3.683(3.669)	0.197	0.247(0.214)
^{90}Zr	NL3	4.194	4.308	4.254(4.268)	4.404(4.393)	0.114	0.149(0.126)
	FSU	4.181	4.269	4.242(4.255)	4.364(4.353)	0.088	0.123(0.098)
^{118}Sn	NL3	4.561	4.760	4.636(4.628)	4.835(4.843)	0.199	0.199(0.215)
	FSU	4.559	4.707	4.634(4.625)	4.780(4.788)	0.148	0.147(0.162)
^{132}Sn	NL3	4.643	4.989	4.700(4.705)	5.077(5.074)	0.346	0.377(0.369)
	FSU	4.654	4.925	4.710(4.716)	5.011(5.008)	0.271	0.301(0.292)
^{208}Pb	NL3	5.460	5.740	5.510(5.514)	5.815(5.814)	0.280	0.305(0.300)
	FSU	5.469	5.676	5.519(5.523)	5.749(5.747)	0.207	0.230(0.224)
^{138}Ba	NL3	4.776	5.012	4.827(4.838)	5.100(5.093)	0.237	0.273(0.255)
	FSU	4.775	4.957	4.826(4.837)	5.043(5.035)	0.182	0.217(0.198)
^{158}Dy	NL3	5.039	5.235	5.099(5.098)	5.309(5.311)	0.196	0.210(0.212)
	FSU	5.027	5.172	5.087(5.086)	5.245(5.246)	0.146	0.158(0.160)
^{176}Yb	NL3	5.215	5.497	5.273(5.272)	5.573(5.574)	0.282	0.300(0.302)
	FSU	5.208	5.424	5.266(5.265)	5.498(5.498)	0.215	0.232(0.233)

TABLE II: Proton, neutron, charge, and weak-charge radii (in fm) of a variety of nuclei as predicted by the NL3 and FSU relativistic mean field models. The last two columns display the neutron skin (R_n-R_p) and weak skin (R_{wk}-R_{ch}), respectively. Quantities displayed in parenthesis have been computed without the spin-orbit correction.

the weak-charge radius of ^{138}Ba, ^{158}Dy, and ^{176}Yb amounts to $\approx 0.008\,\text{fm}$, $\approx -0.002\,\text{fm}$, and $\approx -0.001\,\text{fm}$, respectively. Note that whereas the NL3 and FSU predictions for the weak skin of the various nuclei differ significantly, the spin-orbit contribution appears to have very little model dependence. In general, we find that the intrinsic structure of the nucleon leads to a weak skin that is larger than the corresponding neutron skin. Moreover, for light neutron-rich nuclei—such as ^{22}O and ^{48}Ca—the spin-orbit contribution generates a further enhancement of the weak skin. In particular, whereas the FSU interaction predicts a neutron skin in ^{22}O of $R_{\text{nskin}} = 0.417\,\text{fm}$, the prediction for the experimentally measurable weak skin is significantly larger, namely, $R_{\text{wskin}} = 0.487\,\text{fm}$. Although not as large, the effect is still significant in ^{48}Ca ($R_{\text{nskin}} = 0.197\,\text{fm}$ and $R_{\text{wskin}} = 0.247\,\text{fm}$) and even in ^{208}Pb ($R_{\text{nskin}} = 0.207\,\text{fm}$ and $R_{\text{wskin}} = 0.230\,\text{fm}$). We also display some of these results in graphical form in Fig. 2 where predictions for the weak skin—with and without spin-orbit contributions—are shown as a function of the corresponding neutron skin. Again, the neutron skin is interesting as it represents a pristine nuclear-structure observables that is instrumental in constraining the isovector sector of the nuclear density functional. The weak skin, on the other hand, although sensitive to the internal structure of the nucleon, is both experimentally accessible as well as strongly correlated to the neutron skin. Note that in Fig. 2 we have added the line $R_{\text{wskin}} = R_{\text{nskin}}$ to indicate that in all cases (except for ^{118}Sn) the weak skin is larger than the neutron skin—and significantly larger for the lighter neutron-rich nuclei. Finally, the fact that the points are more "compressed" in the case of FSU than NL3 is a reflection of the softer symmetry energy of the former relative to the latter.

IV. CONCLUSIONS

A relativistic mean-field approximation has been used to compute proton, neutron, charge, and weak-charge densities and form factors of a variety of neutron-rich nuclei. Special emphasis has been placed on the impact of spin-orbit currents on the electroweak skin of these nuclei. Although closely related to the neutron skin, the weak skin—defined as the difference between the experimentally accesible weak- and electromagnetic-charge radii—is sensitive to the internal structure of the nucleon. The weak-charge radius of a nucleus is closely related to the (point) neutron radius because the weak charge of the neutron is much larger than that of the proton. This is analogous to the reason why the charge and proton radii are closely related. In the absence of spin-orbit corrections, and regardless of the model, we found a weak skin larger than the neutron skin for all nuclei investigated here.

Once spin-orbit currents were incorporated, a significant increase in the weak skin—especially in the case of the two lighter nuclei ^{22}O and ^{48}Ca—was observed. In particular, we found quite generally that the spin-orbit contribution
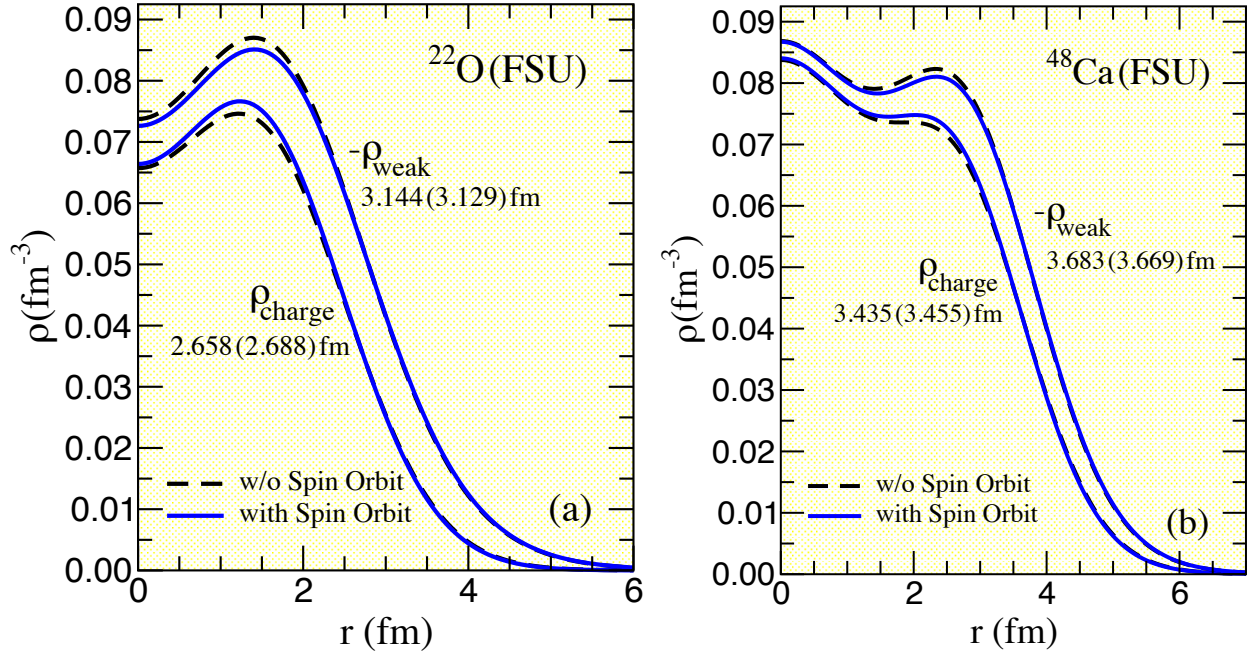
FIG. 1: (Color online). Charge and weak-charge densities for ^{22}O (a) and ^{48}Ca (b) as predicted by the FSU interaction. The dashed lines represent the corresponding densities in the absence of spin-orbit corrections.

to the weak and charge radii enter with opposite sign so their impact is enhanced when computing the weak skin. For example, in the case of ^{48}Ca the spin-orbit enhancement amounts to about 0.03 fm; this is commensurate with the projected accuracy of the C-REX experiment. The impact of the spin-orbit contribution decreases with increasing mass number, so its effect in ^{208}Pb is small (0.006 fm) and well below the proposed ± 0.05 fm accuracy. The spin-orbit contribution is in general small due to the strong cancellation between spin-orbit partners and between neutron-proton pairs in identical single-particle orbits. Given that it lacks the coherence displayed by the dominant (vector) contribution, spin-orbit currents have the largest impact on light neutron-rich (or proton-rich) nuclei with unpaired spin-orbit partners, as in the case of the $1f_{7/2}$ neutron orbital in ^{48}Ca. We note that in the RMF case where the cancellation among spin-orbit partners is incomplete, there is a further enhancement (of about 30%) relative to the non-relativistic predictions due to the presence of a strongly attractive scalar potential (the so-called "$M^\star$-effect").

In summary, accurately calibrated relativistic mean field models have been used to compute the impact of spin-orbit currents on the electroweak skin of a variety of nuclei. Given that spin-orbit contributions to both the charge and weak-charge radii may be significant and often as large as existent or projected experimental uncertainties, spin-orbit currents should be routinely incorporated into future calculations of both charge and weak-charge form factors.

Acknowledgments

Appendix: Single-nucleon electroweak currents

In terms of the underlying quark vector currents, the electromagnetic and weak neutral currents displayed in Eq. (4) are given by the following expressions [25]:

$$\hat{J}^\mu_{EM} = \sum_{f=1}^3 Q_f \bar{q}_f \gamma^\mu q_f = \frac{2}{3}\bar{u}\gamma^\mu u - \frac{1}{3}\bar{d}\gamma^\mu d - \frac{1}{3}\bar{s}\gamma^\mu s, \tag{A.1a}$$

$$\hat{J}^\mu_{NC} = \sum_{f=1}^3 g_v^f \bar{q}_f \gamma^\mu q_f = g_v^u \bar{u}\gamma^\mu u + g_v^d \bar{d}\gamma^\mu d + g_v^s \bar{s}\gamma^\mu s, \tag{A.1b}$$
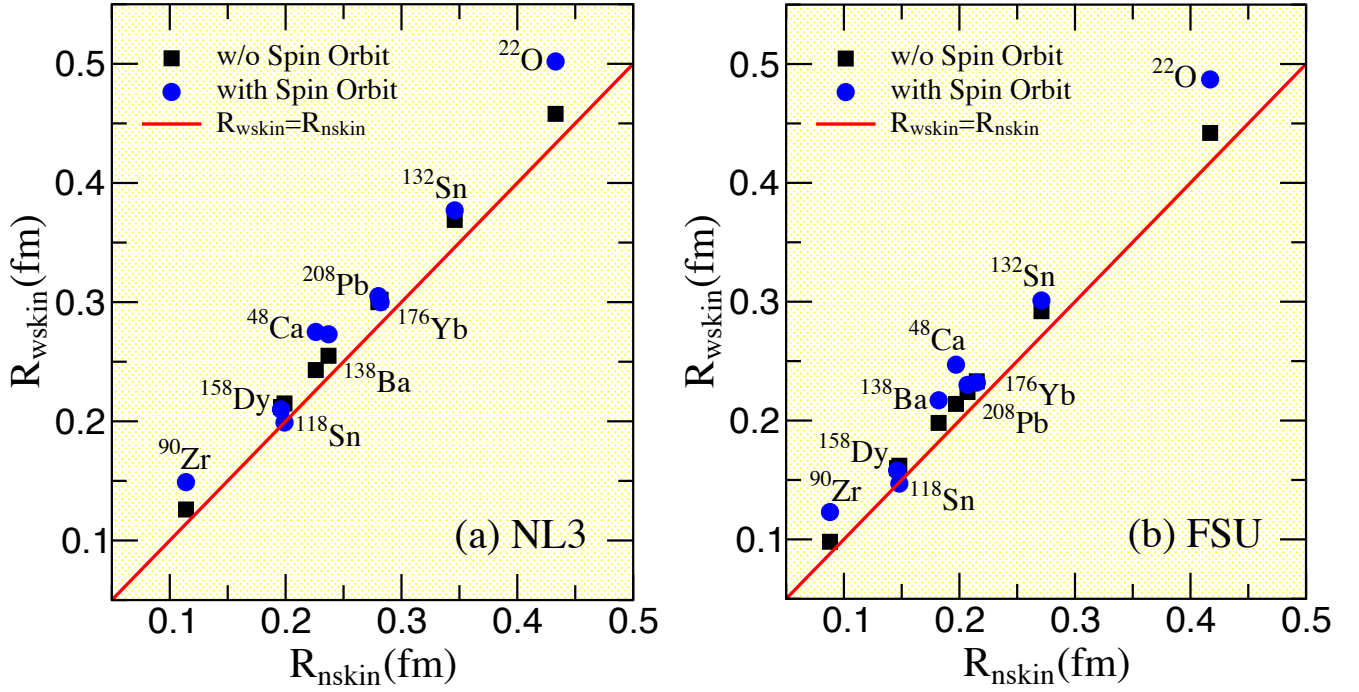
FIG. 2: (Color online). Electroweak skin (R_{wk}-R_{ch}) with and without spin-orbit corrections as a function of neutron skin (R_n-R_p) for the various neutron-rich nuclei considered in this work. Predictions are made using both the NL3 (a) and FSU (b) interactions.

where g_v^f is the weak-vector charge of quark "f" expressed in terms of its weak isospin and the weak mixing angle. That is,

$$g_v^f = 2T_3^f - 4Q_f \sin^2\theta_w = \begin{cases} +1 - \frac{8}{3}\sin^2\theta_w \simeq +0.384 & \text{if } f=\{u,c,t\}, \\ -1 + \frac{4}{3}\sin^2\theta_w \simeq -0.692 & \text{if } f=\{d,s,b\}. \end{cases} \tag{A.2}$$

Note that we are assuming that the heavy-quark (c,b,t) content of the nucleon is negligible. Also note that the weak-vector charge of the quarks are to a good approximation equal to the negative of the electromagnetic charge of its weak isospin partner. This is the main reason why the neutral Z^0-boson is an excellent probe of the neutron density. Assuming isospin invariance, namely, that the up(down)-quark distribution in the proton equals the down(up)-quark distribution in the neutron and that the strange-quark distribution is equal in both, the proton and neutron electromagnetic currents may be written in the following way:

$$J_{EM}^\mu(p) \equiv \langle p|\hat{J}_{EM}^\mu|p\rangle = \frac{2}{3}V_u^\mu - \frac{1}{3}V_d^\mu - \frac{1}{3}V_s^\mu, \tag{A.3a}$$

$$J_{EM}^\mu(n) \equiv \langle n|\hat{J}_{EM}^\mu|n\rangle = \frac{2}{3}V_d^\mu - \frac{1}{3}V_u^\mu - \frac{1}{3}V_s^\mu, \tag{A.3b}$$

where V_u^μ, V_d^μ, and V_s^μ are matrix elements of the respective quark vector currents in the proton. From the above equations one can determine V_u^μ and V_d^μ in terms of the two electromagnetic currents and V_s^μ. That is,

$$V_u^\mu = 2J_{EM}^\mu(p) + J_{EM}^\mu(n) + V_s^\mu, \tag{A.4a}$$

$$V_d^\mu = J_{EM}^\mu(p) + 2J_{EM}^\mu(n) + V_s^\mu. \tag{A.4b}$$

In turn, these relations may be used to express the matrix elements of the weak neutral current in terms of the corresponding matrix elements of the electromagnetic current plus the strange-quark contribution. Inserting these relations into Eq. (A.1b) one obtains:

$$J_{NC}^\mu(p) = g_v^p J_{EM}^\mu(p) + g_v^n J_{EM}^\mu(n) + \xi_v^{(0)}V_s^\mu, \tag{A.5a}$$

$$J_{NC}^\mu(n) = g_v^n J_{EM}^\mu(p) + g_v^p J_{EM}^\mu(n) + \xi_v^{(0)}V_s^\mu, \tag{A.5b}$$

where proton, neutron, and *singlet* weak-vector charges are given—including radiative corrections—by [32],

$$g_v^p = 2g_v^u + g_v^d = (1 - 4\sin^2\theta_w)(1 + R_v^p) \approx 0.0712\,, \tag{A.6a}$$

$$g_v^n = g_v^u + 2g_v^d = -(1 + R_v^n) \approx -0.9877\,, \tag{A.6b}$$

$$\xi_v^{(0)} = g_v^u + g_v^d + g_v^s = -(1 + R_v^{(0)}) \approx -0.9877\,. \tag{A.6c}$$

Note that these values are very close to the ones used in Ref. [2] which are the ones that have been adopted here (*i.e.*, $g_v^p = 0.0721$ and $g_v^n = -0.9878$). Finally, electric and magnetic Sachs form factors for the weak neutral current may be expressed in terms of the corresponding electromagnetic form factors plus the strange-quark contribution as follows:

$$\widetilde{G}_{E,M}^p(Q^2) = g_v^p G_{E,M}^p(Q^2) + g_v^n G_{E,M}^n(Q^2) + \xi_v^{(0)} G_{E,M}^s(Q^2)\,, \tag{A.7a}$$

$$\widetilde{G}_{E,M}^n(Q^2) = g_v^n G_{E,M}^p(Q^2) + g_v^p G_{E,M}^n(Q^2) + \xi_v^{(0)} G_{E,M}^s(Q^2)\,. \tag{A.7b}$$

In particular, using these relations we obtain the following expressions for the nucleon weak-charge radii:

$$g_v^p \tilde{r}_p^2 = g_v^p r_p^2 + g_v^n r_n^2 + \xi_v^{(0)} r_s^2\,, \tag{A.8a}$$

$$g_v^n \tilde{r}_n^2 = g_v^n r_p^2 + g_v^p r_n^2 + \xi_v^{(0)} r_s^2\,. \tag{A.8b}$$

Similar expressions follow in the case of the nucleon weak magnetic moments:

$$\tilde{\mu}_p = g_v^p \mu_p + g_v^n \mu_n + \xi_v^{(0)} \mu_s\,, \tag{A.9a}$$

$$\tilde{\mu}_n = g_v^n \mu_p + g_v^p \mu_n + \xi_v^{(0)} \mu_s\,. \tag{A.9b}$$

Note that the mean-square strange radius and strange magnetic moment are defined as

$$r_s^2 = -6 \frac{dG_E^s(Q^2)}{dQ^2}\bigg|_{Q^2=0} \quad \text{and} \quad \mu_s = G_M^s(Q^2=0)\,. \tag{A.10}$$

[1] S. Abrahamyan, Z. Ahmed, H. Albataineh, K. Aniol, D. Armstrong, et al., Phys. Rev. Lett. **108**, 112502 (2012).
[2] C. J. Horowitz, Z. Ahmed, C. Jen, A. Rakhman, P. Souder, et al., Phys. Rev. **C85**, 032501 (2012).
[3] C. J. Horowitz, Phys. Rev. **C57**, 3430 (1998).
[4] X. Roca-Maza, M. Centelles, X. Viñas, and M. Warda, Phys. Rev. Lett. **106**, 252501 (2011).
[5] C. J. Horowitz, S. J. Pollock, P. A. Souder, and R. Michaels, Phys. Rev. **C63**, 025501 (2001).
[6] I. Angeli, At. Data Nucl. Data Tables **87**, 185 (2004).
[7] K. Paschke, K. Kumar, R. Michaels, P. A. Souder, and G. M. Urciuoli (2012), URL `http://hallaweb.jlab.org/parity/prex/prexII.pdf`.
[8] J. Mammei, R. Michaels, K. Paschke, S. Riordan, and P. A. Souder (2012), URL `http://hallaweb.jlab.org/parity/prex/c-rex/c-rex.pdf`.
[9] J. Piekarewicz, B. Agrawal, G. Colò, W. Nazarewicz, N. Paar, et al. Phys. Rev. **C85**, 041302(R) (2012).
[10] S. J. Pollock, E. N. Fortson, and L. Wilets, Phys. Rev. **C46**, 2587 (1992).
[11] T. Sil, M. Centelles, X. Viñas, and J. Piekarewicz, Phys. Rev. **C71**, 045502 (2005).
[12] M. B. Tsang et al., Phys. Rev. Lett. **92**, 062701 (2004).
[13] L.-W. Chen, C. M. Ko, and B.-A. Li, Phys. Rev. Lett. **94**, 032701 (2005).
[14] A. W. Steiner and B.-A. Li, Phys. Rev. **C72**, 041601 (2005).
[15] D. V. Shetty, S. J. Yennello, and G. A. Souliotis, Phys. Rev. **C76**, 024606 (2007).
[16] M. B. Tsang et al., Phys. Rev. Lett. **102**, 122701 (2009).
[17] C. J. Horowitz and J. Piekarewicz, Phys. Rev. Lett. **86**, 5647 (2001).
[18] C. J. Horowitz and J. Piekarewicz, Phys. Rev. **C64**, 062802 (2001).
[19] C. J. Horowitz and J. Piekarewicz, Phys. Rev. **C66**, 055803 (2002).
[20] J. Carriere, C. J. Horowitz, and J. Piekarewicz, Astrophys. J. **593**, 463 (2003).
[21] A. W. Steiner, M. Prakash, J. M. Lattimer, and P. J. Ellis, Phys. Rept. **411**, 325 (2005).
[22] B.-A. Li and A. W. Steiner, Phys. Lett. **B642**, 436 (2006).
[23] H. Ito and F. Gross, Phys. Rev. Lett. **71**, 2555 (1993).
[24] A. Ong, J. Berengut, and V. Flambaum, Phys. Rev. **C82**, 014320 (2010).
[25] M. Musolf, T. Donnelly, J. Dubach, S. Pollock, S. Kowalski, et al., Phys. Rept. **239**, 1 (1994).
[26] B. D. Serot and J. D. Walecka, Adv. Nucl. Phys. **16**, 1 (1986).
[27] B. G. Todd-Rutel and J. Piekarewicz, Phys. Rev. Lett **95**, 122501 (2005).
[28] J. J. Kelly, Phys. Rev. **C66**, 065203 (2002).
[29] K. Nakamura et al. (Particle Data Group), J. Phys. G **G37**, 075021 (2010).
[30] G. A. Lalazissis, J. Konig, and P. Ring, Phys. Rev. **C55**, 540 (1997).
[31] G. A. Lalazissis, S. Raman, and P. Ring, At. Data Nucl. Data Tables **71**, 1 (1999).
[32] J. Liu, R. D. McKeown, and M. J. Ramsey-Musolf, Phys. Rev. **C76**, 025202 (2007).